International Conference on Space Optics—ICSO 2018

Chania, Greece

9–12 October 2018

Design study of a hosted Arctic imager for weather and climate monitoring in the polar regions

Peter Buschkamp

Stephan Gulde

Charlotte Bewick

Patrick Tully Peacocke

et al.

Design Study of a Hosted Arctic Imager for Weather and Climate Monitoring in the Polar Regions

Peter Buschkamp*[a], Stephan Gulde[a], Charlotte Bewick[b],
Patrick Tully Peacocke[a], Paolo Sandri[a], Frank te Hennepe[b]
[a] OHB System AG, Oberpfaffenhofen, Germany; [b] OHB System AG, Bremen, Germany

ABSTRACT

A Hosted Arctic Imager (HAI) concept is currently being investigated as part of ESA's Polaris program. HAI intends to fulfil the needs for providing weather and atmospheric services in the polar regions enabling e.g. near-real-time observations of Atmospheric Motion Vectors of the Arctic and Nordic regions, similar to the measurements offered by its Meteosat counterparts in GEO, such as SEVIRI on MSG and FCI on MTG. The compact hosted-payload multi-spectral imager operates from a High Elliptical Orbit in 12 spectral bands from 0.4µm to 13.3µm at a Ground Sampling Distance of 1-3km. The optical concepts employs a split design into a wavelength-optimized VIS and a (N)IR telescope, built as all-metal free-form optics, where a hole in the first mirror of the (N)IR telescope presents the entrance aperture of the VIS telescope. Our instrument design maximizes the re-use of heritage technology, e.g. for detectors, scanner, and calibration elements, in order to enable a low-risk fast-track development program.

Keywords: Multi-spectral Imager, atmospheric monitoring, free-form optics, metal optics

1. INTRODUCTION

Interest in the Arctic region has steadily increased in recent years with the use of economic, political, military and scientific arguments. Further, the polar regions have a significant impact on weather and climate on global level, and hence the modelling thereof. Despite its important role, the Arctic region only receives limited satellite-based services because typical GEO or LEO satellite missions have limited spatio-temporal observation capabilities for full Arctic disc coverage and regarding (fast) repeat cycle, ground-sampling pattern and observation angle.

To tackle these challenges, OHB System has supported ESA in an extended Phase0 study, investigating the potential of a two spacecraft mission each carrying a Hosted Arctic Imager (HAI) flying in a Highly Elliptical Orbit (HEO). Similar to the well-known Molniya systems, the spacecraft will spend a significant part of its orbital period in the apogee region with access to the high latitudes effectively covering the Arctic region.

HAI shall provide similar observation services of the Arctic polar region as its counterparts in GEO – such as SEVIRI on MSG and FCI on MTG – do for the lower latitudes, for example near-real-time observations of Atmospheric Motion Vectors.

Consequently, HAI's spectral channel coverage and radiometric accuracy requirements are essentially identical to those of FCI covering the wavelength range from 0.4µ to 13.3µ at 1-3km Ground Sampling Distance. At the same time the mass of HAI shall be no more than about half that of FCI – a main challenge to the design. We have developed an optical instrument architecture which is lightweight and easy to manufacture. Our instrument design maximizes the re-use of heritage technology, e.g. for detectors, scanner and calibration elements, in order to enable a low-risk fast-track development program.

This paper introduces briefly the mission context and provides an analysis of the observational requirements and conditions. We show how the particularities of the Highly Elliptical Orbit, translate into scanning and viewing capability requirements for the HAI instrument. The main focus of the paper lies on the opto-mechanical architecture, which is based on an innovative single 4-mirror telescope design. We show the specific on-board calibration design and provide an outline of the overall instrument design and budgets.

*peter.buschkamp@ohb.de; phone 49 8153 4002-162; fax 49 8153 4002-940; www.ohb-system.de

2. MISSION CONTEXT

2.1 Mission goals

HAI has been defined as a multi-spectral imager with the following high-level requirements:
- o   Observation area: land and sea surfaces > 55° northern latitude and local inst. View Zenith Angle < 63°
- o   Observe the observation area for a time frame of 9.5 h per orbit centred around the apogee passing
- o   Instrument boresight shall be pointed towards the North Pole
- o   Provide a full scan of the observation area (or the observable part thereof) every 10 minutes
- o   Observe the observation area in 12 optical channels, among which are:
   2 visual channels, 1 high spatial resolution panchromatic visual channel (HRV)
   1 near-infrared channel, 3 mid-wave infrared channels, 5 thermal infrared channels
- o   Observe the observation area with a Ground Sampling Distance (GSD) of 3 km at the reference viewing configuration for all channels, except for the HRV with a GSD of 1 km.

2.2 Orbit and observation geometry

To identify all boundary conditions to the instrument design, a thorough analysis of the orbit has been performed. This includes an investigation of the impact on the observational geometry and the Sun intrusion angle. Figure 1 shows an illustration of the orbit geometry. The selected orbit is a so-called Three Apogee (TAP) orbit, which has an orbital period of 16 hours, and in order to ensure continuous service coverage, the system shall consist of two satellites. In order to avoid rotation of the argument of perigee, the critical inclination (63.4°) is selected and the apogee is placed over the northern hemisphere. An important parameter in the analysis of the observation geometry is the angle α, which is defined as the rotational angle around the instrument boresight axis of the instrument reference frame with respect to the Earth fixed reference frame, see Figure 4.

Orbit parameter	Value
Apogee altitude	43509 km
Perigee altitude	8089 km
Orbital period	57600 s
Eccentricity	0.55
Inclination	63.4°
Argument of perigee	270°
RAAN	65°
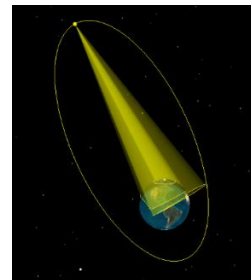
Figure 1. Illustration of the orbit geometry and orbital parameters

To analyse the change in the zone of interest as seen from the satellite, we modelled the imaging area as the intersection of the zone of interest (> 55° northern latitude) and the View Zenith Angle constraint (VZA < 63°). Figure 2 plots the change in zone of interest and geometry of the imaging area over the course of an orbital period. In this figure, the instrument Field of Regard is presented in black, which is defined as the viewing range accessible to the scanning instrument and limited by the Earth baffle. At any point during the observation period, deep space is visible within the field of view for background calibration.
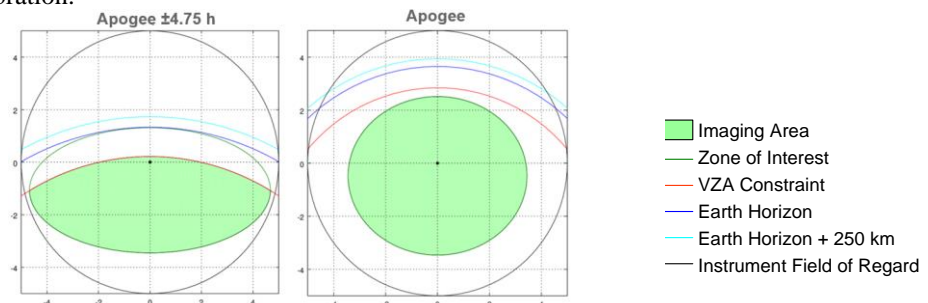
Figure 2. Change of imaging geometry in the zone of interest over an orbital period.

2.3 Observation concept: Scanning

In order to cover the complete zone of interest within the required update interval of 10 minutes, the instrument will make use of a line scanning concept. A detailed trade-off comparing different scan concepts (line-scan vs. step-and-stare) and possible detector solutions has been performed to select the line scanning concept. While both concepts require similar aperture sizes, focal length and thus number of detector arrays, the StepStare concept requires an optical instantaneous field-of-view (IFOV) ~4 times larger than the Line Scan concept. In the StepStare concept, the instantaneous field-of-view (IFOV) of the instrument is shaped as a 1D-line of pixels and a complete image (repeat cycle) is acquired by sweeping this IFOV using a whisk-broom concept over the zone of interest. Figure 3 shows the scanning concept selected for HAI.
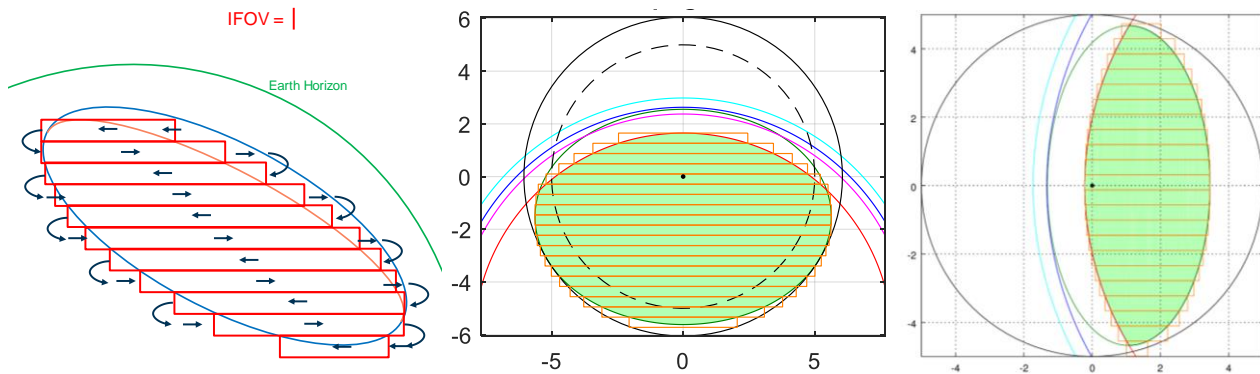
Figure 3. Illustration of the scanning concept (left) and imaging pattern of the zone of interest (middle $\alpha =0°$, right $\alpha=90°$). Imaging area in green, VZA constraint: red line, earth horizon: cyan, imaging FOV: black, imaging lines: red rectangles

The line scanning concept allows the re-use of the FCI 1D-line detectors. By combining the scanning concept with the zone of interest, one can analyse the imaging pattern caused by scanning behaviour. The result of this analysis is shown on the right hand side of Figure 3. A parametric analysis of the number of line segments and the total length of the scanning line was computed as function of orbit time. The results are presented in Figure 4.

Total line length
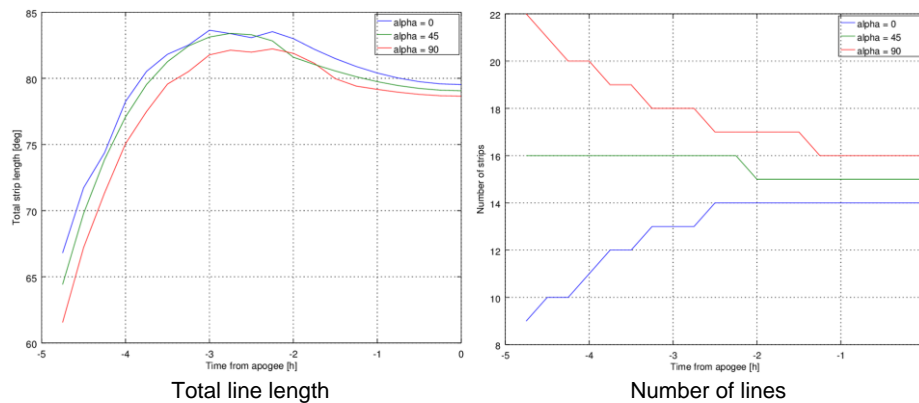
Number of lines

Figure 4. Behavior of the HAI scanning concept parameters

The rotational angle α does not significantly affect the total imaging line length but leads to an increase in the number of line segments. Furthermore, the largest imaging area is encountered at the start of the operational phase and decreases steadily until apogee.

3. PAYLOAD

3.1 Payload block diagram

The HAI instrument has been designed to have a compact, modular and stiff structure. The main design drivers are:

- High modularity
- Minimal footprint on the bus platform (hosted payload)
- Lightweight + Stiffness
- Materials compatibility (CTE + cleanliness)
- Thermal and mechanical decoupling
- Baffle-Integrated calibration mechanism
- Easy manufacturability / AIT / Optical alignment / Harness installation
- Use of existing technologies

The Earth baffle has been designed with a baffling angle of 10°, such that any incident Sunlight (arriving at 22° incidence angle in worse case) does not hit any internal HAI elements. For the scanning mechanism, a single mirror with a 2-axis gimbal mechanism has been selected. The HAI instrument is divided into the following modules:

Optical Instrument Module (OIM), containing the opto-mechanical-thermal part of the instrument
Control Electronics Module (CEM), containing the complete set of control electronics units
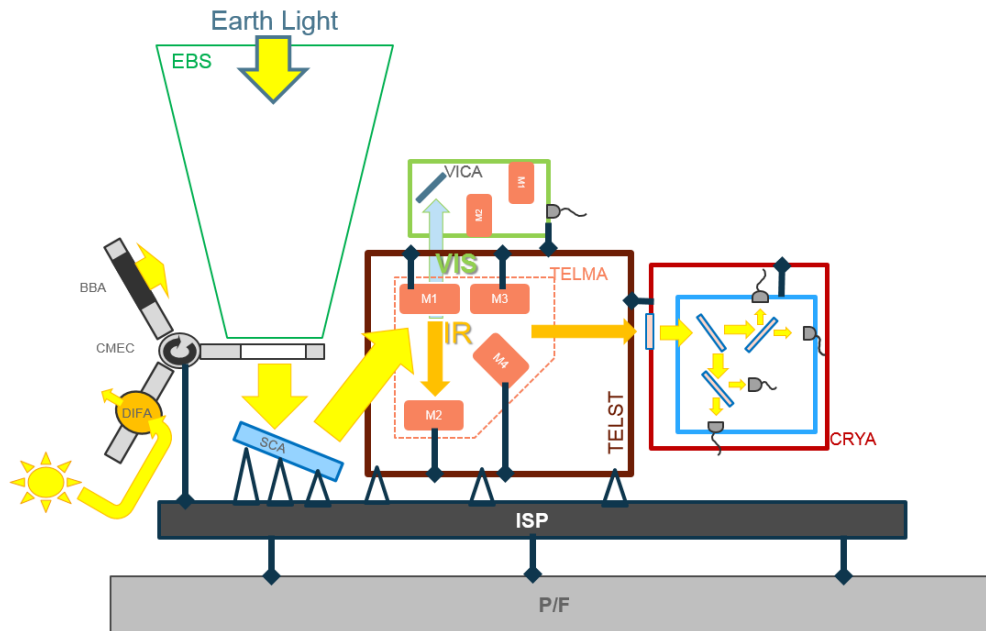
Figure 5. Block diagram of the instrument payload. All instrument components are mounted on a common instrument service panel (ISP) that attaches to the platform. See text for details.

Figure 5 shows the block diagram of the instrument payload. All OIM and CEM modules attach to an Instrument Support Panel (ISP). This ISP connects to the platform. Looking at Figure 5, the Earth light enters the earth baffle structure (EBS) from the top. Before being reflected by the scanner assembly (SCA) it passes the calibration mechanism (CMEC, shown in open position). The CMEC features three ports, one open position for normal operations and two calibration sources, a black body (BBA) and a solar diffuser assembly (DIFA). The scanner assembly reflects the light into the telescope structure (TELST) housing the 4-mirror Infrared telescope assembly (TELMA). The VISUAL channel with its telescope assembly (VICA) is located on the back of the main telescope structure. Light enters the VICA through a circular aperture in the IR telescope's first mirror. The VICA also holds the VIS focal plane system (FPS). Infrared light passes through the IR telescope, exiting on M4 and entering the cryostat assembly (CRYA). The CRYA consists of an outer warm and an inner cold box, holding the cold dichroic and the four cold IR-FPS.
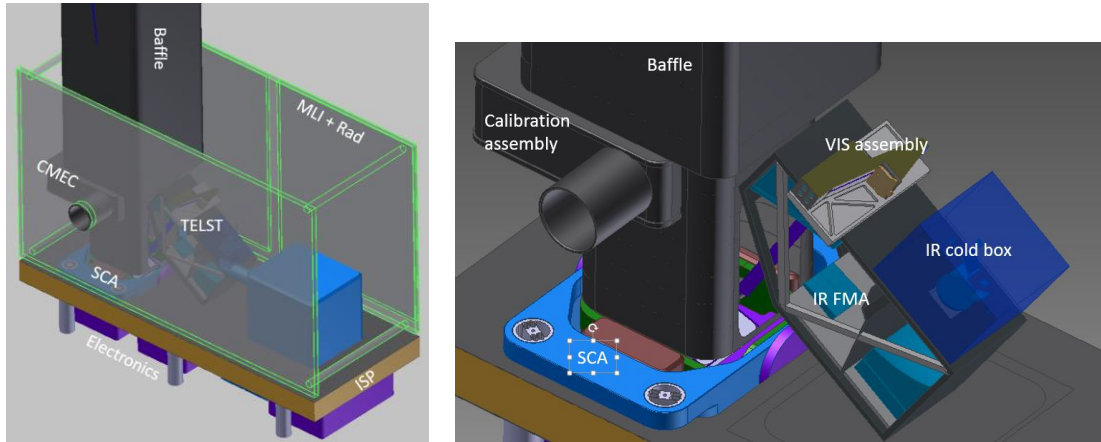
Figure 6. (left) overview of the payload, (right) 3D close-up view of the baffle, calibration, scanner and telescope assembly. Conceptual drawing, support and other structures not shown.

Figure 7 shows the thermal concept. The HAI instrument is equipped with two separate radiators, which are dedicated to the IR cold box, incl. cryo-cooler and the control electronics. Both radiators are positioned on the –y-panel due to absence of incident Sunlight onto this side throughout the mission lifetime. The effects of Earth radiation on the radiators, in particular around perigee was found not to impact the required thermal stability.
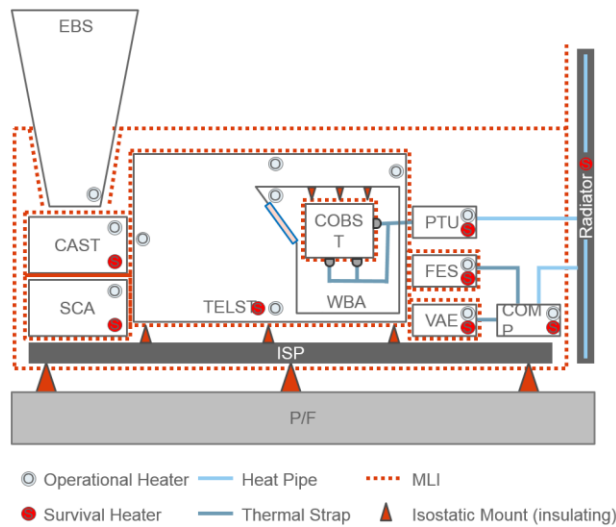
Figure 7. Block diagram of the instrument thermal concept.

Based on the previously described baseline design, the key figures for the HAI instrument are reported in Table 1. All values include an equipment and a flat system margin.

Table 1. Key characteristics of the HAI instrument

Instrument mass	203.6 kg
Instrument volume	1.2 m^3
Instrument envelope	1 m x 1.5 m x 2 m
Average instrument power in Earth observation mode	436 W
Generated data rate	2.8 Mbps

3.2 Optical Design

The HAI optical design is characterized by a split of the optical path after the scan mirror into two telescopes. A 2-mirror VIS telescope and a 4-mirror telescope for all the (N)IR channels. The (N)IR telescope features an accessible field stop for stay-light suppression. Both telescopes are focusing, there are no separate cameras. This is afforded by the following design:

- The VIS channel passes through the central hole in the primary mirror M1 of the (N)IR Telescope. This central hole acts also as the VIS entrance pupil;

- The VIS channel features a separate new telescope, which looks through the hole in the primary mirror M1.

- All the other spectral bands (NIR & IR1-3) use a common 4-mirrors front telescope, followed by a common cryostat with cold beam-splitters for the separation of the four infrared channels.
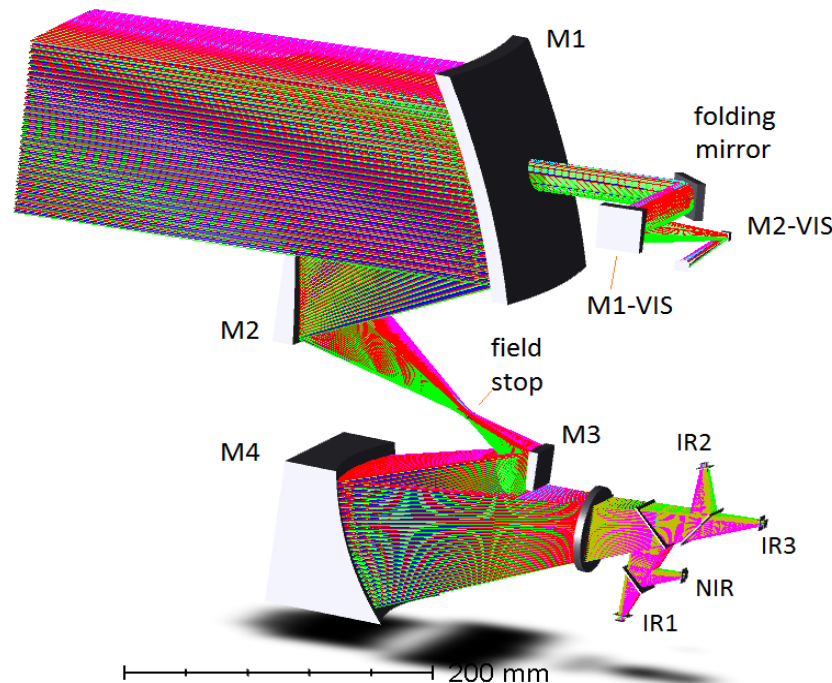
Figure 8. 3D view of the optical layout. Thickness of the mirror substrates shown is arbitrary and for visualization only.

This design approach has the following advantages:

- Relaxed surface polish of TEL mirrors from ~ 0.5nm (RMS) for a common (VIS + (N)IR telescope) to about ~ 1.5-2 nm (RMS). Since the main telescope is in this design only needed for wavelength >1360nm instead of >414nm, we can allow for a ~3 times higher surface roughness σ to achieve the same scattered light performance.

- The coating of the IR Telescope Mirrors can be protected gold, which is much better suited for NIR and IR bands where the reflectivity is >~97% over the whole (N)IR range

- The Scan mirror stays compact and will have (FCI-like) enhanced silver coating. Its surface roughness is ~0.8nm RMS

- No VIS-NIR beam splitter needed. Consequently, the IR cryostat window does need no tilt as it does not double as a beam splitter. Thus the windows it is also smaller. It can be built as a simple plane parallel ZnSe window with only an AR coating. The wave front error is also reduced.

- The cryostat for the NIR focal planes can be much simpler and smaller having only one entrance port.

- ▪ Easier non-astigmatic optical I/F between the (N)IR Telescope and the cryostat assembly.

- ▪ The VIS channel can be built as a simple piece of optics; it is much easier to align as it has its own independent optical train. VIS throughput is also higher since it can be VIS optimized and does not need to pass unnecessary mirrors as in the case of a combined VI-IR telescope.

Obviously, the proposed approach introduces some challenges. A separate VIS telescope independent from the IR will show some impact on spatial co-registration. Further, the primary mirror of the IR telescope needs to be manufactured with a central hole acting as the aperture stop for the visible telescope. This hole can however be fairly small (~20mm) while still be being compliant to MTF requirements. However, the inner wall of the hole and a small coronal area surrounding the hole need to be blackened.

The IR Telescope

The F/2.5 IR telescope consists of four off-axis mirrors. All the four powered surfaces are even aspheres that share the same optical axis. The entrance aperture has a square shape. The incoming rays are reflected by a flat scan mirror toward the primary mirror of the telescope. As discussed above, this scan mirror is common to the IR Telescope and the VIS telescope. The IR-telescope has an intermediate focal plane where a rectangular field stop can be placed. After mirror M4, a plano-parallel window made of ZnSe identifies the window of the cryostat. The aperture stop of the telescope is placed just behind the cryostat window and acts as a cold stop. The aperture stop is parallel to the window of the cryostat. Then the rays travel toward a dichroic #1 which reflects the wavelengths of the NIR and IR1 bands and transmits the wavelengths of IR2 and IR3 bands. The dichroic #2 reflects the wavelengths of the IR2 band and transmits the wavelengths of the IR3 band. The dichroic #3 reflects the NIR band and transmits the IR1 band. The three dichroic plates are made of ZnSe with an inner edge of a few arcmin to compensate for transversal aberrations. In front of each image plane there is a plano-parallel window acting as a filter made of germanium, except for the NIR band which has a filter made in fused silica. The primary mirror features a central hole with diameter ~20 mm. This hole represents the aperture stop for the visible channel. The hole is drawn with an outward conical shape toward the rear side of M1 to avoid vignetting of the rays of the visible channel and minimizing at the same time potential stray-light effect. The actual shape of the hole is optimized taking into account the manufacturing aspects of the mirror. Figure 9 shows the mirrors conceptually without apertures, this allows to see that the four mirrors share the same optical axis.
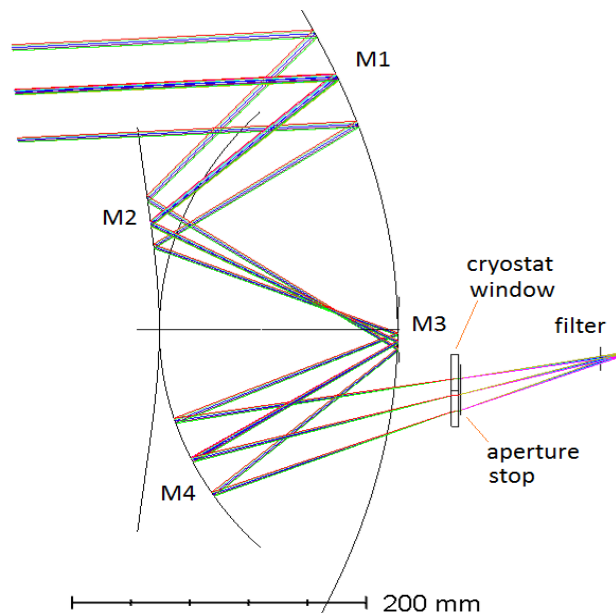
Figure 9. Sectional view of the telescope without apertures to show that the four mirrors share the same optical axis.

The shapes of the mirrors drawn in Figure 8 and 9 are conceptual. An optimization of the shape taking into account the manufacturing aspects has been performed. Figure 10 shows the spot diagrams of the IR telescope at 1.36µm (left) and 12.3µm (right) compared to the Airy disc.
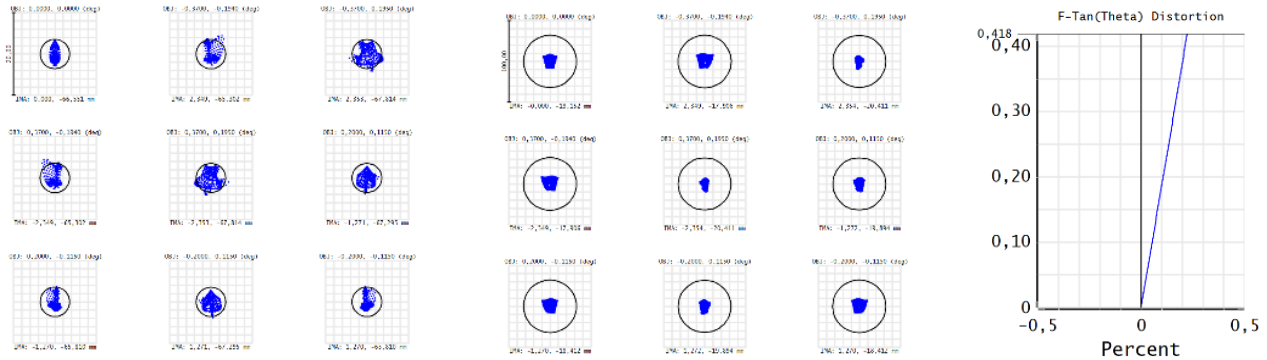
Figure 10. Spot diagrams of the IR telescope at 1.36µm (left) and 12.3µm (middle). The scale bars are 20µm and 40µm respectively Right: plot of geometric distortion

Figure 11 reports the MTF curves as a function of the spatial frequency in 1/km at 1.36µm and 12.3µm respectively. The MTF curves are plotted it in terms of GSD via $\nu_{ground} = \nu_{detector} * f * GSD / D_{ref}$ where ν_{ground} is the frequency in unit of 1/GSD on ground, $\nu_{detector}$ the frequency at detector in 1/mm unit, f the focal length, D_{ref} the reference altitude and GSD the ground sampling distance. GSD = 3km and D_{ref} =43496km.
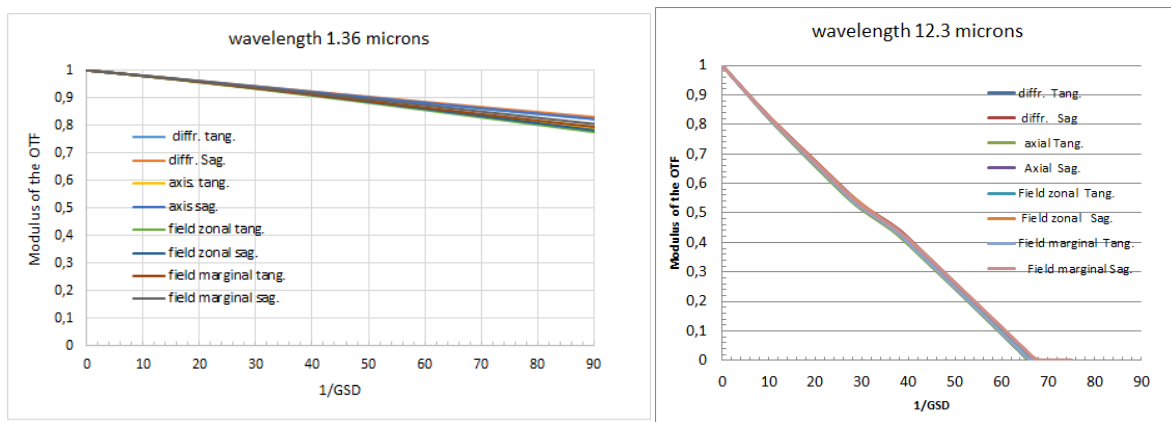
Figure 11. MTF curves at 1.36µm and 12.3µm

Impact of the hole in M1

The manufacturing of a central hole on the primary mirror M1 of the telescope generates a coronal area of few millimeters around the hole where the surface form of the mirror M1 will be slightly degraded. To evaluate the impact on the nominal performances of the IR telescope by adding a hole in the center of the primary mirror we report in Figure 12 the diffractional MTF curves at the wavelength of 12.3 µm calculated with a hole on M1 presenting a diameter from 20 mm to 28 mm. It can be seen that a small (e.g. 1-2 mm) radial aperture around the hole has minimal impact on the MTF.
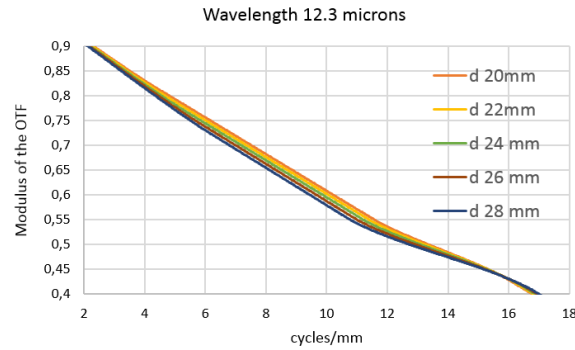
Figure 12. Diffractional MTF curve at 12.3 µm for a central obstruction of the mirror with diameter from 20 mm to 28 mm.

Manufacturability of the IR telescope & the hole in M1

The central hole in the primary acts as the aperture stop for the visible channel, which is placed behind the mirror M1. Thus the hole must be a) as sharp as possible boundaries to reduce stray light problems, b) the hole shall have a cone-like structure to prevent vignetting of the rays of the field of view of the visible channel and to prevent grazing incident light that might be reflected into the visible channel, and c) the hole shall not degrade the surface form error of the mirror M1. The actual manufacturing of the hole, specifically the trade of the technologies used, is an ongoing bread board study.

Achievable manufacturing tolerances have been checked against tolerances derived from a Monte Carlo analysis of the telescopes design parameters. The design is well within state-of-the-art manufacturing tolerances. To reduce alignment errors and to improve manufacturability we explored the possibility of manufacturing M1+M3 and/or M2+M4 on the same or a common substrate to facilitate AIT. Figure 9 indicates that a common substrate of M1+M3 should be feasible. A detailed manufacturing tooling analysis of a fitting free form shows that in fact it is.

A Common substrate for M2+M4 is harder to achieve. Shifting M4 towards M2 results in pupil stretching. This however can be controlled by taking a free form approach to the respective optical surfaces. Alternatively we explored a back-pack approach as shown in Figure 13, where M1 and M3 are manufactured on a common substrate and M4 is snapped onto an enlarged M2 substrate. See also [1] for a similar approach.
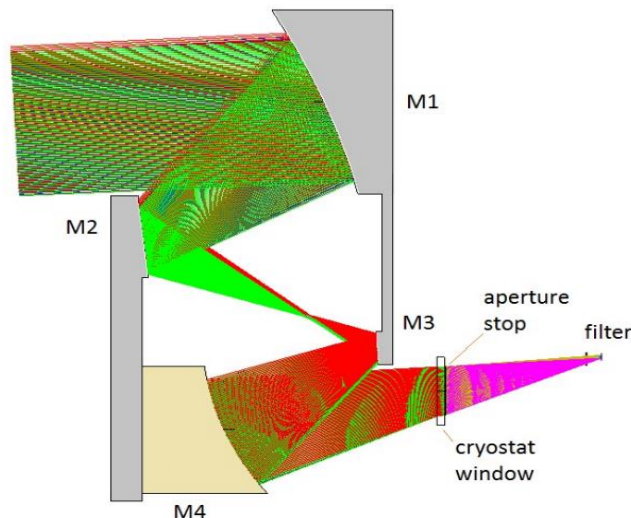
Figure 13. Couple of mirrors M1+M3 (same substrate) and M2+M4 ("back-pack"). Conceptual drawing.

A possible residual lateral misalignment of M2 and M4 was found to be well within the tolerances adopted in the telescope design parameter Monte Carlo analysis.

The VIS Telescope

The visible telescope is located behind the primary mirror of the IR telescope. Figure 14 shows the layout of the chosen all-reflective design. The aperture stop is placed in the hole of mirror M1 of the IR telescope. The telescope is a Cassegrain-like design slightly modified, with only two powered mirrors. The all-reflective layout presents the advantage of being very compact, achromatic and with an athermal behavior when manufactured in aluminium alloy as for example AlSi42, the same material of the IR telescope
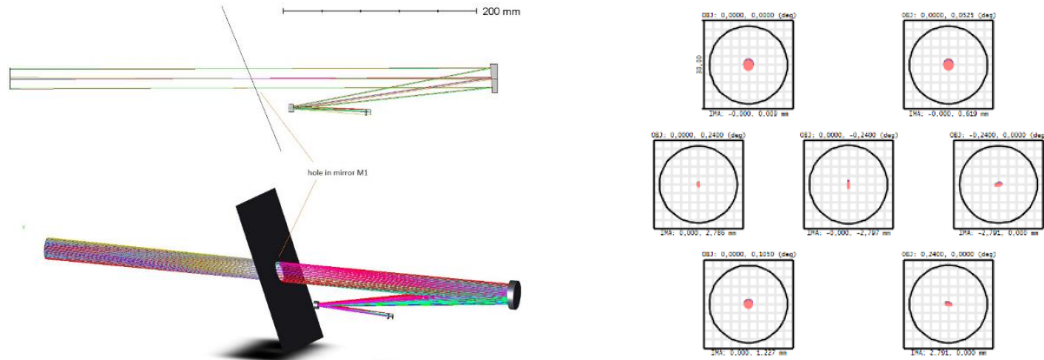
Figure 14. VIS telescope layout (left) and spot diagram (right), geometric spot radius ~2µm.

SYSTEM MTF

The following figures show the nominal MTF performance for some system channels. The baseline design is compliant to the nominal MTF requirement specification in all channels with comfortable margin.
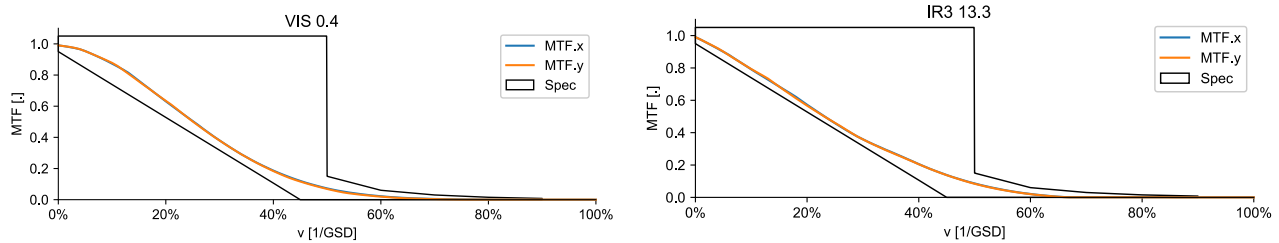
Figure 15. MTF curves for 0.4 and 13.3µm

Due to the fact that the aperture shape is different - it is square with a circular obscuration in the middle for the infrared and a circular Aperture for the VIS channel - the MTF curves show a different shape. This can be seen best when comparing the contributor breakdown for the VIS high resolution channel and the longest IR 13.3µm channel, note the "kink" in the diffraction contributor (compare figure 12)
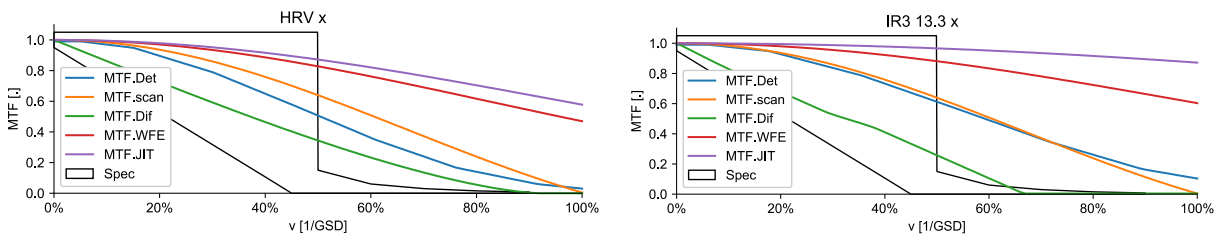
Figure 16. Comparison of the MTF contributors for the High Resolution VIS channel (HRV) and the 13.3µm channel.

3.3 Focal Plane Concept

For the HAI focal plane design selection, it has been decided to re-use the MTG FCI-detectors. In view of schedule, risk and cost aspects a 1:1 rebuild of the FCI detectors regarding ROIC and pixel architecture (lithography) is envisaged. Regarding the spectral filters, which are part of the FCI detector assemblies, moderate adjustments have been considered in order to meet the HAI spectral channel specifications, which differ in some aspects from the FCI ones.

The VIS detector is developed by e2v in CMOS technology while the other 4 detectors, NIR, IR1, IR2 and IR3, are developed by Sofradir in Mercury Cadmium Telluride (MCT) technology. Each detector consists of several pixel columns (between 2 and 5 columns), which are well separated and independent of each other. Every column addresses a single spectral channel. The detector retinas without any filter or window in front are rather broadband in their spectral response. The actual fine selection of a spectral channel is implemented by stripe-like optical pass-band filters positioned directly in front of the pixel columns. In case of the NIR/IR detectors the cut-off wavelength of the MCT is adjusted to the spectral channel from detector to detector, and in some cases (IR1 and IR3) even within one detector.

Each spectral channel column is not just a simple line of adjacent square pixels in single file, but a rather complex pattern of rhombus shaped pixels. This is illustrated in Figure 17 by a zoom into the VIS detector as an example. Yet, the architectural concepts shown here are the same for the NIR and IR detectors. As can be seen in this figure, each channel consists of 4 specially nested columns of rhombus pixels. This 4-fold redundancy leads to an effectively defect-free detector on the level of a spectral channel. The physical dimensions of the pixel rhombus (c_x and c_y) are individually optimized for each channel in order to compensate for different effects: a) there is compression along x, i.e. $c_x < c_y$. This compensates System MTF for the image smear occurring in scan direction (x). This enables a homogenous System MTF in the spatial dimension, i.e. the values for System MTF in along-track direction (x) and across-track direction (y) are equalized. b) Each channel has a different global pixel size: c_x and c_y get smaller with longer wavelength in order to compensate System MTF for optical diffraction. This enables a homogeneous System MTF in spectral dimension, i.e. the values for System MTF in different spectral channels are equalized.
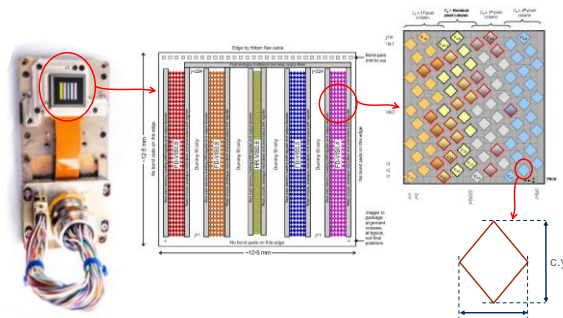
Figure 17. Insight into the architecture of the FCI detectors here: FCI VIS detector (with contributions from [2] and [3])

3.4 Calibration concept

Apart from the necessary on-ground calibrations prior to launch and additional calibrations (e.g. in-flight geometric or radiometric calibrations, such as star-viewing or moon-viewing vicarious calibrations), the main in-flight calibrations, are background calibration, sun calibration and blackbody calibration. These require dedicated flight H/W or have influence on flight H/W, and are included in the HAI baseline.

Background calibration aims to calibrate the signal offset, i.e. the zero-scene-signal of the instrument. For the IR channels (IR1-IR3) this needs be done by full aperture deep space viewing, as any physical instrument piece to which (part of) the aperture would point would by creating a false background signal corresponding to the instrument's own temperature. Calibration has to be done with a relatively high repetition frequency (15min, or better faster) because of radiometric stability. A medium-fast repetition frequency (~1/orbit) is sufficient for VIS & NIR background calibration because thermal background radiation is negligible in the VIS & NIR. These channels are rather dominated by detector dark current variation (by detector temperature instability) which is much less severe than in the IR channels. Thus we focus on providing a full aperture deep space view (mainly for IR), which shall be accessible all the time during operational phase of the orbit.

Sun calibration is necessary for high-signal calibration for the VNIR channels. It needs to be performed with a medium-to-low repetition frequency (1/orbit or 1/day). Sun intrusion angle calculations and FoV considerations show that sun calibration needs a dedicated solar port pointing 90degrees off the Earth baffle that includes a diffusing element and couples into the normal optical path.

Blackbody calibration is used for high-signal calibration for IR-channels. It is performed at a medium repetition frequency (1/h to 1/orbit).

Figure 18 shows the block diagram of the calibrations assembly. All calibration functionalities are provided by the same unit consisting of a wheel mechanism that is inserted in the optical beam in front of the scanner.
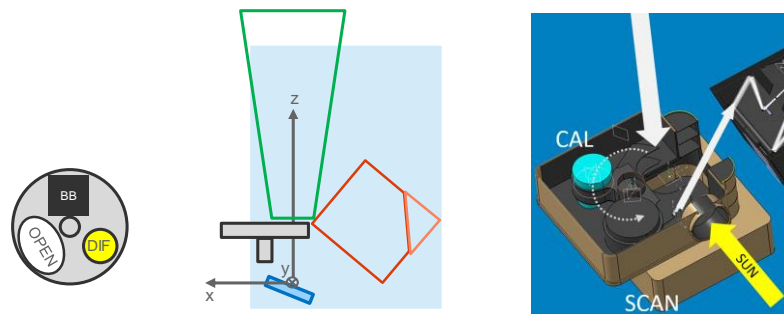
Figure 18. (left, middle) block diagram of the calibration unit. The wheel is shown in grey, earth baffle in green. The red box denotes the main optics assembly on the –x side of the cal assembly (right) 3D view together with the main optics assembly

As is illustrated in Figure 18, the calibration assembly supports the following three wheel positions:
- Position 1: Open for imaging of the nominal scene (Earth viewing)
- Position 2: Diffusing element for Sun calibration via the Sun calibration port
- Position 3: Blackbody elements for blackbody calibration

In addition, the wheel also provides the shutter functionality for the sun port. The BB position has also shutter functionality for the Earth Baffle port. This means that no additional aperture cover mechanism is needed. A very small Scanner range of only 2.5° mechanical scan radius (for Earth coverage) is needed with the employed calibration assy which is a significant operational advantage.

4. PERFORMANCE ASSESSMENT

4.1 Spectral and Spatial sampling

In order to fulfil all observational requirements, the Hosted Arctic Imager acquires samples in 12 spectral channels. In Table 2, the spectral and spatial characteristics of these channels are shown.

Table 2. Spectral and spatial performance characteristics of the HAI channels

Channel number	Channel name	λ_{center} (µm)	bandwidth (µm)		GSD-x (km)	GSD-y (km)
1	HRV	0.7	0.44		1.00	1.00
2	VIS 0.6	0.64	0.08		2.00	2.00
3	VIS 0.8	0.865	0.05		2.00	2.00
4	NIR 1.6	1.610	0.05		3.00	3.00
5	IR 3.8	3.800	0.400		1.50	1.50
6	IR 6.3	6.300	1.000		3.00	3.00
7	IR 7.3	7.350	0.500		3.00	3.00
8	IR 8.7	8.700	0.400		3.00	3.00
9	IR 9.7	9.660	0.300		3.00	3.00
10	IR 10.5	10.500	0.700		1.50	1.50
11	IR 12.3	12.300	0.500		3.00	3.00
12	IR 13.3	13.300	0.600		3.00	3.00

Thanks to the selected solution based on FCI heritage, up to 4 additional detector columns are available in the baseline design (VIS 0.4, VIS 0.5, NIR 1.3, NIR 2.2), which could be used for additional spectral channels. The performance has been evaluated at the reference viewing configuration, which is defined as satellite at apogee, with the target at sub-satellite point. Furthermore, the reached GSD values refer to the L0 data recorded by the instrument. With this spatial performance, it is possible to easily implement a homogenous GSD of 3 km across all channels in the on-ground L1 data processing by suitable co-addition.

4.2 Radiometric Noise

The radiometric background signal as, for example, generated by detector dark current and thermal background radiation varies in time. Furthermore, the background calibration measurement has its own noise. These two effects (background variation and background calibration imperfection) could be interpreted as noise in a sense of system SNR (VIS & NIR) or NEdT (IR channels), and this is a matter of noise definition. We distinguish between:

a) „Classical noise" which is the high frequency radiometric error fluctuation, fully uncorrelated even between direct neighbor pixel of an image. Main origins of classical noise are shot noise and read-out noise. We use the suffix "classic" for the SNR/NEdT which is obtained from classical noise alone.
b) Radiometric background variation as described above. We use the suffix "backvar" for the SNR/NEdT which is obtained when interpreting the background variation effects as noise.

In the following, we report these different noise figures individually ("classic" & "backvar") as well as their sum effect.

Table 3. Radiometric Noise performance achieved by the HAI Orbit#2 baseline versus HAI Radiometric Noise requirement

	Channel	VIS 0.4	VIS 0.5	HRV	VIS 0.8	VIS 0.6	NIR 1.3	NIR 1.6	NIR 2.2
SNR specified	SNR.spec [one]	25	25	25	21	30	40	30	25
Achieved SNR per L1 sample, i.e. after 2D (xy) spatial coaddition to the spatial sampling	SNR.L1.classic [one]	71	65	49	63	84	282	325	107
Effective SNR produced by background variations, combining temperature deviation effects and their calibration.	SNR.backvar [one]	2579	2045	2661	2160	3270	16246	19017	5549
Total SNR per L1 sample, counting both, classical noise and temperature deviation effects.	SNR.L1.all [one]	71	65	49	63	84	282	325	107

	Channel	IR1 3.8	IR1 6.3	IR1 6.9	IR2 8.7	IR2 7.3	IR3 10.5	IR3 12.3	IR3 13.3
	NEdT.spec [K]	0,10	0,30	0,30	0,10	0,30	0,10	0,20	0,50
Achieved L1 NEdT (when viewing Lref) Note: This is counting only classical noise	NEdT.L1.classic [K]	0,0202	0,0055	0,0075	0,0055	0,0089	0,0081	0,0231	0,0328
Effective NEdT produced by background variations, combining temperature deviation effects and their calibration via dark sky views	NEdT.backvar [K]	0,0002	0,0007	0,0007	0,0009	0,0025	0,0027	0,094	0,130
Total NEdT per L1 sample, counting both, classical noise and temperature deviation effects.	NEdT.L1.all [K]	0,0202	0,0056	0,0076	0,0055	0,0092	0,0086	0,096	0,134

In summary the baseline Radiometric Noise performance is compliant with moderate to good margin in the VIS (VIS 0.6 being slightly worse) and is compliant with generous margin in the NIR_1.6 channel and in all IR channels.

5. CONCLUDING REMARKS

Using the results of the feasibility study, ESA is taking the next steps in the form of a follow-up system consolidation activity. Supporting the existing meteorology line of WMO, EUMETSAT and NOAA, HAI will in this way represent a promising means to augment the weather and climate monitoring activities in the Arctic and Nordic regions should a flight opportunity materialize.

We have shown that a compact and lightweight hosted-payload multi-spectral imager can be realized using all-metal free-form optics. All components are backed by technologies of at least TRL 5 (mostly 6-7). The re-use of heritage technology where possible enables a lower-risk fast-track development program.

OHB System acknowledges the support and funding from ESA for the realization of the activity.

6. REFERENCES

[1] S. Risse, et al., "Development and fabrication of a hyperspectral, mirror based IR-telescope with ultra-precise manufacturing and mounting techniques for a snap-together system assembly", Proc. Of SPIE Vol. 8176, 81761N-1, 2011

[2] S. Demigual, et al., "MTG FCI Visible Detector Detection Chain Description and Preliminary Results", International Conference on Space Optics 2014, Tenerife, Canary Islands, Spain, October 7 - 10, 2014

[3] P. Pidancier, et al., "Sofradir Detectors for MTG FCI Application", International Conference on Space Optics 2014, Tenerife, Canary Islands, Spain, October 7 - 10, 2014

[4] F. te Hennepe, et al., „Weather and climate monitoring in the arctic regions", 68. International Astronautic Congress 2017, IAC-17-B1.2.3, Adelaide, Australia, 2017